Deep Space Atomic Clock
Technology Demonstration Mission Results

Todd Ely, John Prestage, Robert Tjoelker, Eric Burt, Angela Dorsey, Daphna
Enzer, Randy Herrera, Da Kuang, David Murphy, David Robison, Gabriella
Seal, Jeffrey Stuart, Rabi Wang
Jet Propulsion Laboratory, California Institute of Technology
4800 Oak Grove Dr.
Pasadena, CA 91109-8099
Todd.A.Ely@jpl.nasa.gov

Jill Seubert
1321 Upland Dr. PMB 1104
Houston, TX 77043-4718

Abstract — The Deep Space Atomic Clock (DSAC), a NASA
Technology Demonstration Mission, was launched into low-
Earth orbit on June 25, 2019 as a hosted payload aboard
General Atomics' Orbital Test Bed (OTB) spacecraft. The
DSAC mission has been conducting a two-year demonstration
of a mercury ion atomic clock to characterize its space-based
performance and to validate its utility for deep space navigation
and radio science.

Analysis of the collected data using JPL's GIPSY-OASIS
software has shown DSAC's AD at one-day to be near 3×10^{-15};
much better than required AD of 2×10^{-14}. Such low spacecraft
clock errors will enable one-way radiometric tracking data with
precision equivalent to or better than current-day two way
tracking data, allowing a shift to a more efficient and flexible
one-way deep space navigation architecture. To verify this, an
analog deep space navigation experiment was performed using
JPL's operational navigation software (Monte). The experiment
recovered orbit solutions with reduced data sets and geometric
variations that are more representative of deep space missions,
and showed that orbit determination using DSAC derived data
is on par with more traditional two-way datatypes.

As a technology demonstrator, DSAC's development focus has
been on maturing the mercury ion trap clock technology rather
than achieving the smallest size, weight, and power (SWaP).
Over the course of DSAC's development the project has
identified numerous improvements that could be made to
significantly reduce SWaP for DSAC's next version. Indeed,
DSAC-2 was recently selected by NASA for further
demonstration on the VERITAS mission to Venus.

This work will review the DSAC technology, mission, and
results from its two-year mission.

TABLE OF CONTENTS

1. INTRODUCTION

NASA's Deep Space Atomic Clock (DSAC) Technology
Demonstration Mission (TDM) is a low Earth orbiting
payload that launched June 19, 2019 and began mission
operations on August 18, 2019. The DSAC TDM's primary
objective was to characterize the space-based performance of
an advanced prototype mercury ion (^{199}Hg$^+$) atomic clock and
to validate its utility for future deep space navigation and
radio science. The over two-year mission completed
operations on September 18, 2021.

Current deep space navigation depends primarily on ground-
based atomic clocks for the formation of accurate two-way
coherent radiometric measurements. Until DSAC, space-
based clocks have lacked the stability necessary for most
deep space navigation needs based solely on one-way
radiometric signals. Navigating with typical space clocks
(such as an Ultra Stable Oscillator or USO) using one-way
tracking data has had limited use because of the correlation
between long-term frequency drift and orbital parameters.
That is, solving for large clock bias and drift terms following
long periods with no tracking significantly degrades the orbit
solution quality. DSAC has the potential to bridge the gap
between ground and space clocks, beginning with the current
mission's validation of its on-orbit performance and
demonstrating that its long-term stability is in family with
that of the Deep Space Network (DSN). The Allan deviation
(AD) of DSAC is required to be less than 2×10^{-14} at one-day.
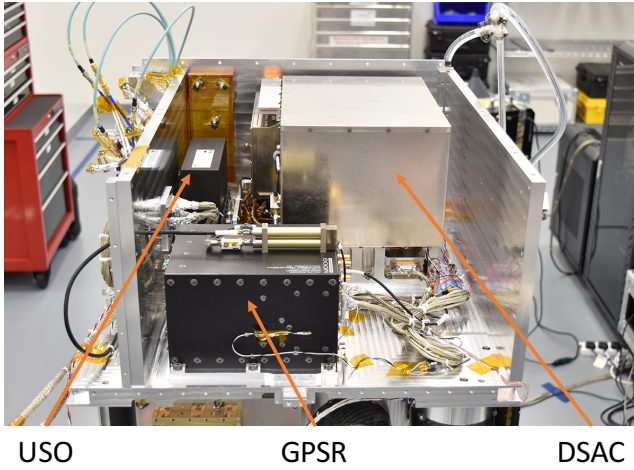
USO   GPSR   DSAC

Figure 1: The DSAC payload integrated onto OTB's middeck payload bay.

As recently reported by Burt, et al. [1] and highlighted later in this paper, DSAC achieved a stability of 3×10^{-15} at one-day. Such low spacecraft clock errors are enabling for one-way radiometric tracking data with precision equivalent to and, in some cases, better than current two-way tracking data. Indeed, this success has led to NASA's selection of a follow-on DSAC demonstration (dubbed DSAC-2) to be hosted on NASA's VERITAS mission to Venus that is planned for launch later this decade. DSAC-2 will be a smaller, longer lived mission ready version of a mercury ion clock that will make it ideally suited for infusion into future NASA mission, DoD missions, and even commercial applications.

Hosting DSAC on board a spacecraft coupled with its frequency stability across integration times relevant to navigation and radio science enables precision one-way radiometric tracking that opens up an array of benefits, notable examples include:

1. Flexible navigation operations with potential to support unlimited users in a single DSN antenna beam, and fundamental to future satellite positioning systems beyond Earth. See Ely, et al. [2] and [3] for examples and details.

2. Autonomous radio navigation needed for extended 'lights out' operations. Autonomous navigation is critical to future human exploration of the solar system, could reduce risks to extended aerobraking operations, enable for future satellite tours of the outer solar system, and/or improve the accuracy of planetary flyby/entry navigation. See Ely, et al. [4] for a detailed case study of how this could work for navigating to Mars.

3. Radio science with 10–100 times more accurate data that could be used for gravity recovery, radio occultations of planetary atmospheres, or even tests of relativity [5].

The DSAC payload consists of several key components including the DSAC Demonstration Unit (DU), the USO supplied by Frequency Electronics, Inc. (FEI), a Moog Broad
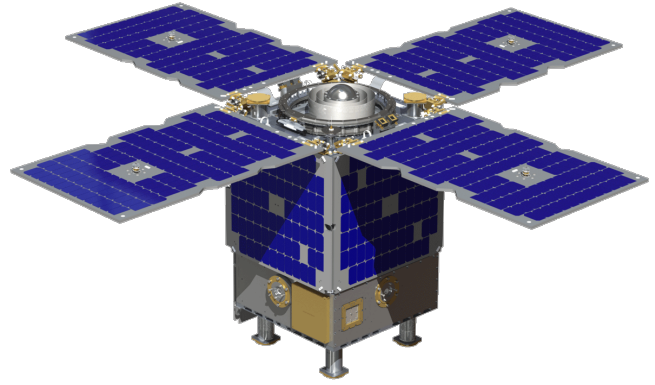

Figure 2: OTB spacecraft in its on-orbit configuration (figure provided by General Atomics).

Reach TriG Global Positioning System receiver (GPSR), and GPS choke ring antenna. The DSAC payload is hosted onboard General Atomics' Orbital Test Bed (OTB) spacecraft. Figure 1 shows the DSAC payload integrated into OTB's mid-deck payload bay. Because DSAC is a technology demonstrator, the development focus has been on maturing the mercury ion trap clock technology and not to achieve the smallest size, weight, and power (SWaP). Nonetheless, DSAC SWaP (including both the DU and USO) is modest at approximately 19 L, 19 kg, and 56 W. Over the course of DSAC's development the project identified numerous improvements that will be applied to the development of DSAC-2, which will significantly reduce these values without sacrificing performance.

OTB (Figure 2) was manifested on the US Air Force's Space Technology Program 2 (a SpaceX Falcon Heavy rocket), and launched on June 25, 2019 into a 720 km altitude, near-circular orbit with an inclination of 24°. OTB nominally maintains the DSAC payload's GPS antenna in a zenith orientation that allows for a continuous view of the GPS constellation and collection of L1 and L2 carrier phase and pseudo-range data by the GPSR using DSAC as its external reference. The GPS data, along with payload and spacecraft telemetry, was transmitted to an Earth ground station (operated by ViaSat) and then to the JPL-based DSAC investigation team via GA's Mission Operations Center. The DSAC investigation team analyzed all collected telemetry to assess the state of the clock and to determine its stability. JPL's GNSS-Inferred Positioning System and Orbit Analysis Simulation Software (GIPSY-OASIS) was used to reconstruct the orbit, relevant dynamic parameters, and the clock's performance. Additionally, a deep space analog navigation experiment was performed using Monte, JPL's operational deep space navigation software, to recover orbit solutions with reduced data sets and geometric variation more representative of deep space missions. A summary of these results is reported on in this paper.

2. MISSION ARCHITECTURE AND OPERATIONS

The DSAC investigation focused on three key elements:

1. characterize the clock's performance,

2. characterize the clock's state,

3. demonstrate the clock's utility as a navigation instrument.

The clock's performance and orbit recovery were based on processing the collected GPS data to determine the stability of DSAC and the utility of DSAC for navigation. Key tools used to reconstruct the orbit, relevant dynamic parameters, and the clock performance included the GIPSY-OASIS and Monte [6], [7]. Additionally, the GPS orbit and clock solutions from the JPL GNSS Analysis Center were utilized as part of the clock and orbit determination process. The clock's state, operating characteristics, and health were assessed using an extensive set of telemetry data collected from the DSAC payload.

Key DSAC Performance Requirements

The DSAC mission requirement for estimating clock stability (Allan deviation or AD) was less than 2×10^{-14} at one-day, which can be expressed equivalently as < 2 nanoseconds gain/loss in a day. Based on the measured ground performance, the project had a stability goal of < 3×10^{-15} at one-day (or 0.3 nanoseconds/day) and was achieved during the on-orbit testing. Even though the key requirements specify stability at one-day, the project investigated clock performance on a large range of time scales. On shorter time scales below 10 seconds, the stability of the USO driving DSAC is the key performance factor. In the $1 - 10$ second range, the USO has a stability of better than 2×10^{-13}. Fundamentally, the clock control process improves on this stability level over longer time scales and asymptotically approaches a white frequency noise characteristic until it reaches (typically on the order of days) some 'floor' level performance. Indeed, as first reported in Burt, et al. [1], the clock achieved a long-term frequency drift of 3×10^{-16}/day that established a record for a space clock.

With DSAC performing at this level, its utility for one-way radiometric deep-space navigation can be validated by showing that orbit determination performance using the one-way data performs as well as or better than its traditional two-way counterpart. To this end, another key mission requirement was to demonstrate orbit determination uncertainty of less than 10 meters (3 sigma) using one-way radiometric tracking data with measurement quality, quantity, and schedule characteristics (such as track duration and data gaps) that are operationally similar to that available in deep space navigation (dubbed the 'deep space navigation analog experiment'). This was readily achieved as first reported by Seubert, et al. [8] and is summarized later in this paper.

Payload Description

The DSAC payload consists of three sub-systems (and associated cabling):

1. An ovenized crystal Ultra Stable Oscillator (USO) produced by Frequency Electronics Incorporated (FEI) with short term (between $1 - 100$ seconds) stability of at most 2×10^{-13} and frequency drift below 1×10^{-10}/day,

2. The DSAC Demonstration Unit (DU) containing the physics package that monitors the USO output and creates a synthesized, stabilized frequency output,

3. The GPS system is comprised of a JPL-designed TriG-Lite receiver produced by Moog Broad Reach and a zenith-pointing choke ring antenna designed to minimize multipath effects. The TriG receiver is designed to be highly configurable, capable of tracking multiple frequencies from GPS and other GNSS constellations on multiple antennas. For DSAC, the TriG receiver is configured to use one antenna to track up to 16 satellites on GPS L1 and L2 frequencies.

Additionally, the DSAC flight software is resident on the OTB's Payload Interface Unit. During normal clock operation, the USO provides an input frequency to the DSAC DU and the DU calculates corrections to the USO signal to produce a stabilized frequency output. This output signal is then used as the reference for the GPS receiver. The GPS system collects the carrier phase and pseudo-range data from the GPS constellation (see Figure 3) that is later telemetered to the ground for use in the precision clock determination (PCD) process. The DSAC payload of the USO, DU, and GPS receiver reside in the payload bay of the spacecraft located in the mid-section of the spacecraft bus (see Figure 1). The GPS antenna resides on the space-facing panel of the spacecraft (see Figure 2), in a configuration that provides an unobstructed view of the GPS constellation. This enables continuous GPS data collection throughout the mission, excepting GPS receiver resets.

Spacecraft Description

The spacecraft has been designed for nadir pointing. The DSAC space-pointing requirements for the GPS antenna to be zenith-oriented represent a nice complement to that primary attitude. Some other key characteristics of OTB as they relate to DSAC on-orbit investigation follow:

Attitude knowledge and control. The spacecraft provides a relatively stable platform for the DSAC investigation. The spacecraft has no active propulsion system. All deployables (such as the solar arrays) are fixed once deployed. De-orbit at the end of the OTB mission is accomplished via deploying drag chutes to increase drag area. The attitude control system utilizes wheels, gyroscopes, and a magnetic control system with magnetorquers for actuators and a magnetometer for attitude determination. Magnetic effects on the clock, from the magnetorquers and the Earth's magnetic field, have been modeled and measured and do not present a significant error source for DSAC's long-term stability. On a periodic basis, the spacecraft rotates by 180-degrees about the Z-axis (yaw flip) to maximize solar array exposure and minimize the exposure of the spacecraft radiator to the sun in response to seasonal variations in the environment. The clock is expected to operate through these maneuvers. Attitude knowledge is achieved via the magnetometer, gyroscopes, and four sun
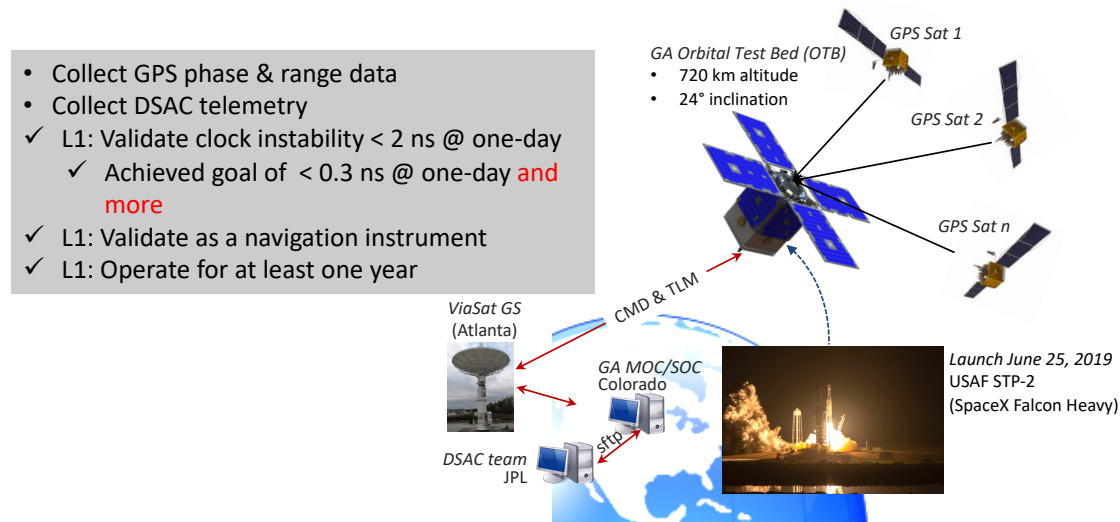
- Collect GPS phase & range data
- Collect DSAC telemetry
- ✓ L1: Validate clock instability < 2 ns @ one-day
  - ✓ Achieved goal of < 0.3 ns @ one-day and more
- ✓ L1: Validate as a navigation instrument
- ✓ L1: Operate for at least one year

GA Orbital Test Bed (OTB)
- 720 km altitude
- 24° inclination

GPS Sat 1
GPS Sat 2
GPS Sat n

CMD & TLM

ViaSat GS
(Atlanta)

GA MOC/SOC
Colorado

sftp

DSAC team
JPL

Launch June 25, 2019
USAF STP-2
(SpaceX Falcon Heavy)

Figure 3: Mission Architecture

sensors. The DSAC team receives the vehicle's attitude history via the same file-based transfer interface used for the DSAC payload and GPS telemetry. This data is available within approximately twenty-four hours of the payload and GPS telemetry.

Thermal. While the spacecraft experienced significant temperature variations throughout the mission and more modest variations during any given orbit, the thermal interfaces to the USO, clock, and GPS receiver have been designed so that the expected thermal variations meet their thermal operational range. There are no specific requirements on thermal control of the cabling between the units or the GPS antenna. A particular thermal sensitivity relevant to the validation system is the GPS receiver's phase sensitivity to temperature variations; however, a precision calibration model was used to correct for this effect with its effects illustrated later in this paper.

Power—Spacecraft power is provided by solar panels. The orientation of the solar panels has been selected to minimize multi-path effects on the GPS antenna, and their configuration is considered in the spacecraft model used by the precision clock determination process. The DSAC payload is required to operate across a wide input voltage range, but DSAC power converters that manage the voltage beyond the interface regulate the applied voltage sufficiently that changes in the input voltage are not a significant factor in the precision clock determination process.

Time—The OTB clock (not DSAC) is used to time-tag all platform telemetry (such as the attitude history). The OTB ground system synchronized the spacecraft on-board clock with a ground-based reference nominally once per day where the ground was synched to UTC using a GPS receiver and a time server. The on-board computer sends that time out periodically to the various spacecraft nodes and other payload units that require it. OTB's payload interface unit also provides timing to the DSAC flight software. The inaccuracies in these time tags relative to GPS time are small

and introduce negligible effects in the DSAC data analysis. (Note that the GPS receiver data is time-tagged using the GPS receiver clock that is stabilized by DSAC). Any discontinuities in the telemetry time-tags with GPS time were be resolved by the DSAC ground system.

Mission Interfaces and Operations

Payload commissioning began August 18, 2019 and on November 6, 2019 official nominal operations commenced with all elements of the DSAC payload powered on, stable, and operating. During operations, the DSAC investigation team at JPL operated the DSAC payload via transmitting commands and receiving data through the GA OTB mission and spacecraft operations center (MOC/SOC) at GA's facility in Englewood, Colorado, which then routed the commands to and received telemetry from OTB using a ground station in Atlanta, GA and operated by ViaSat. As shown Figure 3, the DSAC investigation team used a secure FTP (sftp) server, that is part of the DSAC ground data system (GDS), to interface with the MOC/SOC. Via this interface, the DSAC GDS collected GPS, DSAC telemetry, and selected data from OTB and made it available to the DSAC investigators for analysis.

Five types of data were collected for the DSAC investigation:

1. GPS receiver data (including engineering telemetry and the observables from the GPS constellation) collected nominally on a 10 second interval.

2. Clock telemetry (including housekeeping data, control settings, and clock corrections).

3. Spacecraft data, such as attitude, power, thermal, magnetic and other miscellaneous data related to the state of the platform (or externally-sensed temperature of the payload units) that may be useful in correlating signatures in the clock performance to the environment.

4. GPS constellation orbit and clock solutions,

5. Environment information such solar flux data and Earth orientation data.

The first three data sets were collected by the on-orbit computer and stored in a file format on-board. At least once daily, these files were made available for downlink via an automated downlink process. The GPS constellation orbit and clock solutions used by DSAC were obtained from JPL's IGS Analysis Center (for JPL orbit and clock solutions).

After the data were received on the ground, they were placed on a secure FTP server by the OTB ground system. Nominally, DSAC data were downlinked on one (single) pass per day. The DSAC data downlink volume was designed to fit within a single nominal pass; however, a latency of three days allowed for the event of lost passes or other anomalies that interfered with the nominal downlink. The DSAC ground system retrieved the data from the secure FTP server and delivered it to the DSAC local repository.

A secure FTP server was also the DSAC interface to the OTB uplink process. Command request files were generated by the payload operations team in the form of acquisition schedule XML files. The files allowed specification of the execution time for each command as an absolute or relative time. Acquisition schedules were placed on the secure FTP server at least 4 hours prior to the required execution time on the spacecraft. The OTB ground system reviewed the command requests to confirm they posed no threat to the platform and were consistent with the expected configuration. The DSAC team was notified within a timely manner that the command was accepted for uplink. The OTB ground system was responsible for generation of the uplink products and getting them on-board in time for their earliest execution time. Commanding was available to the DSAC operations team every day, but not needed during nominal clock operations.

Over the course of the two-year mission, most of the calendar time was available to the DSAC mission to operate the payload; however, there were periods of time that OTB encountered faults that forced the spacecraft into safe mode. Standard practice with safe mode is to power down the payloads, including DSAC. None of these events effected DSAC in any physical way, and, in each instance once GA resolved the fault, OTB and DSAC returned to nominal operations. The operations statistics for the duration of DSAC mission, a 760.2-day period from August 20, 2019 04:21:30 (GPS time) to September 18, 2021 03:40:00 (GPS time) are provided in Table 1 below.

Table 1: DSAC Mission Operations Statistics

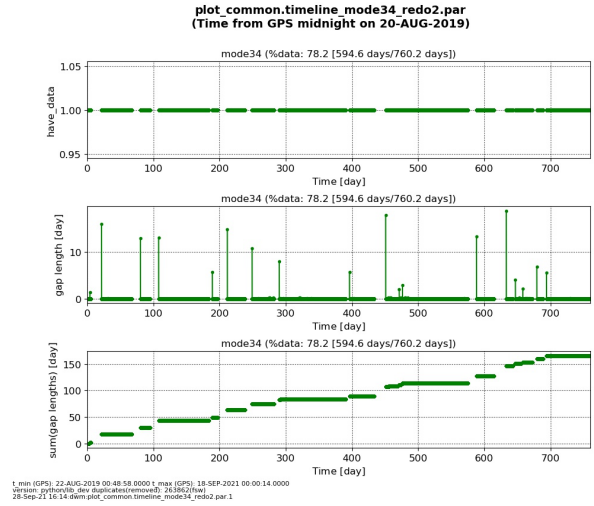| Operational Category	Percent Time Active (760.2-day period)
GPS data collection	74.9%
DSAC in 'clock mode'	78.2%
USO powered on	84.6%

Figure 4: Illustration of the active times when DSAC is in clock mode (top) over the whole mission duration, the length of each gap and when during the mission that DSAC is not in clock mode (middle), and the cumulative sum of these gap times (bottom).

An illustration of the DSAC in clock mode (which is nominally when the clock is locked on the USO a producing a stable output; however, may include unlocked times for the purpose of running tests on the clock) is shown in Figure 4. The figure includes 3 plots with the top illustrating the periods of time that DSAC is actively in clock mode, the middle is the duration of each gap and when it occurs as a function of mission elapsed time, and the bottom is the cumulative sum of these gaps. Collectively, the DSAC mission performed active clock experiments 78.2% of the time for a total of 569.2 days of the 760.2-day mission.

3. DATA ANALYSIS

Numerous types of data were collected from the DSAC payload and OTB and then analyzed. In order to collate and efficiently analyze all the available data, we developed a simple common file format for nearly all data types and implemented file conversion routines to translate original data into the common format. During conversion, all data was assigned a GPS timestamp, aligning the data to a common time scale. In addition, files were consolidated into daily batches. Furthermore, we developed common plotting software that could select, manipulate, and plot common file data for all available time ranges and source files, regardless of the data's time cadence. DSAC analysts used this plotting software either from the command-line or as an automated operational process.

In this section we will describe our nominal operations, the use of the common plotting software to create plots of both clock and spacecraft telemetry, and how the GPS data was processed to verify the clock performance requirement (an Allan deviation of 2×10^{-14} at one-day) and demonstrate the best space-clock performance to date Burt, et al. [1]. Not discussed is our diagnostic mode used to investigate and characterize key clock operation parameters like lamp noise,
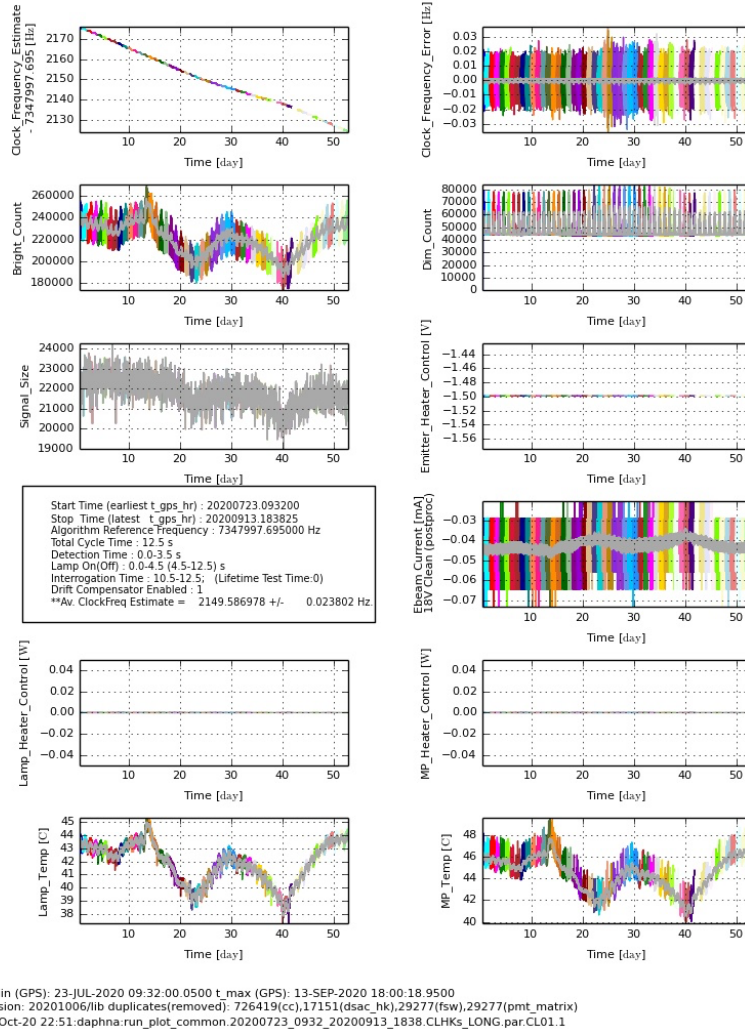
Figure 5: Sample first page clock telemetry plots from DSAC 52-day run reported on in Burt, et. al. [1]**.**

ion load time, resonance line-shape, microwave-power profile, and USO acquisition, for which we have separate analysis and plotting tools.

Nominal Operations

Telemetry was transmitted on a daily basis from the spacecraft to the GA MOC/SOC. These data were continually mirrored, via sftp, from the MOC/SOC to our local operations computer at JPL. From there, an automated process parsed files as they arrived, and converted them into the common file format.

The common plotting software was used to generate daily, weekly, cumulative, and on-demand telemetry plots, in order to track the progress of clock operations and performance throughout the mission. The daily plots allow a closer look at recently downloaded data, while the plots with longer timescales more easily reveal trends and/or changes. Plot pages from our common file plotting software were standardized with header and footer information to clearly

indicate the plot time span, the plotting tool, and the time of creation. We found that standardizing the look and information contained in these plots helped to identify trends and anomalies.

Clock and Spacecraft Telemetry Plotting

During nominal operations, we produced sixteen-page plot packages: nine with basic clock telemetry, two with basic spacecraft telemetry, two with a mixture of clock and spacecraft telemetry to track voltages and temperatures against their alarm limits, and two with specialized clock telemetry analysis plots to monitor detector and lamp noise levels. As an example, Figure 5 shows a sample of telemetry plots (the first page of a set of sixteen) illustrating the 52-day run reported on in Burt, et. al. [1]. The clock is locked, as indicated by the expected *Bright Count* per cycle (PMT counts during the time that the light source is turned on) and *Signal Size* levels. The clock's automated *Signal Size* measurements (indicated by excursions in the Bright Count telemetry stream) interrupt the clock cycle, so are only

conducted intermittently. *Clock Frequency Estimate* indicates the synthesizer frequency control that must be applied to keep the drifting USO and synthesizer locked to the ion resonance. Its plot therefore roughly tracks opposite the USO drift. The other plots on this page show heater power, temperatures, light levels during dim mode (PMT counts when the light source is turned off), electron emitter function, and the control loop error frequency, which tracks to zero over time. The colored sections delineate different days of data, and the grey line through the middle of each plot shows the smoothed version. An approximately 15-day periodic pattern in several of the plots follows or is caused by changes in spacecraft temperature over the 52 days.

Other clock telemetry pages show additional temperatures, microwave probe power level, DC supply voltages, trap voltage and PMT high voltage monitors, averaged signal size values used by the control loop, finer detail of the detected *Bright Count* (plotting 100 ms detection bins rather than full cycles), and more. Plot alignment and layout facilitates the identification of event correlations, if any deviations from nominal occur. Most plots show telemetry fields taken directly from the source data, but some show calculated or derived values. For instance, an optical-pumping-time plot is constructed by fitting an exponential curve to the *Bright Count* 100 milliseconds bin profile for each clock cycle, starting at lamp turn-on, and several Allan deviations are also calculated.

The three spacecraft telemetry pages show supply voltages and currents for the three DSAC payload components (USO, GPS, and the atomic clock package), six external temperature sensors, and the USO oven current. We also combine the supply voltages and currents into calculated power plots to directly monitor power consumption.

Orbit and Initial Clock Determination

During nominal operations, the JPL high-precision orbit determination software packages GIPSY-OASIS is used to determine the DSAC clock error $x(t)$ together with OTB spacecraft orbital position and velocity from on-orbit GPS phase and pseudo-range data in L1 and L2 frequency through the standard ionospheric-free linear combinations of LC (phase) and PC (pseudo-range) observables. Due to the weak measurement geometry and high correlation between receiver clock error parameter and the height component of orbital position, pure geometric/kinematic positioning usually suffers poor quality mapped from random and systematic measurement errors. We use reduced-dynamic orbit determination technique that utilizes the orbit dynamics to augment the measurement geometry while compensating the imperfect dynamic model with estimating stochastic dynamic error time series. This technique was developed at JPL and has been practiced in many missions and improved over last decades (Wu, et al. [9]; Bertiger, et al. [10]).

In addition to the GPS measurements, the measurements of the OTB attitude in space are also used in the orbit determination process for computing the offset between the GPS receiver antenna and the center of mass of the spacecraft; as well as, the GPS carrier phase wind-up effect due to the change of antenna orientation in space. Other auxiliary data and models used in the orbit determination are summarized in Table 2. *A priori* data noise of 1 cm and 1 m are assigned to the LC and PC measurements, respectively. Each daily orbit determination task is performed over a 30-hour arc, leaving 6-hour overlap interval between any two consecutive days.

Table 2: Summary of data and models used in the orbit determination

Model/Data	Approach
GPS constellation orbit and clock	Fix to JPL IGS Analysis Center IGS14 products, 30-hour arc (Dow, et al. [11])
GPS tracking data	30-second dual frequency carrier phase and range
OTB attitude data	8-second quaternion time series
GPS receiver multipath error	Iterative data fit residual map in azimuth and elevation
Earth's gravity models	EIGEN-6S2 200x200 time-varying spherical harmonic model (Förste, et al. [12]), solid Earth tide, ocean tide and pole tide models
Drag	Drag coefficient with DTM-2000 atmospheric density model
Solar Radiation Pressure	8-panel S/C body model with surface optical properties
Empirical Accelerations	1 cycle per revolution in cross- and along-track; 1, 2, and 3 cycle per day in along-track; 3-D stochastic accelerations at 30-second rate.
Reference frame	IGS14 with geocenter location estimated (Kuang, et al. [13])

The GPS observables were analyzed using a reduced dynamic model (RDM) filter to perform the orbit determination. The RDM filter uses spacecraft dynamical acceleration states that account for force modeling errors via tuned stochastic ECRV accelerations as summarized in Table 3. The process is iterated to generate a converged solution. Note that in the first part of the mission extended data sets were used to determine a calibration model for the receiver multipath errors with the resulting maps are shown in Figure 6. Final orbital position and clock error estimates are evaluated in difference between the 6-hour overlapping interval of two neighboring orbital arcs.

The average RMS of 3D orbital position overlap difference is 0.80 cm. The average RMS of clock $x(t)$ overlap difference is 3.0 cm. However, the average standard deviation of clock

overlap difference is 0.89 cm, consistent with the orbital position error. This means that the dominant part of the clock overlap difference is a bias at the day boundary between the two daily solutions (possibly due to the fact that relativity correction is not applied in the orbit determination). This day boundary difference is eliminated in later y(t) calculation and does not affect the evaluation of Allan Deviation.

Table 3: RDM Filter Configurations

Estimated Parameter	Type	A Priori sigma	Process Noise
Initial Position (J2000)	Dynamic	100 km	
Initial Velocity (J2000)	Dynamic	1 km/s	
Drag Coefficient	Bias	1.0e3	
SRP Scale	Bias	1.0	
Periodic (H, C, L) Accel	Bias	1.0e6 μms^{-2}	
Stochastic (H, C, L) Accel.	ECRV	(10, 10, 15) nms^{-2}	$q = \sigma^2(1 - e^{-2\Delta t/\tau})$ $\sigma = (2, 5, 10)$ nms^{-2}, τ = 30 s, Δt = 30 s
Clock Offset	WN	1 s	$q = \sigma^2$, Δt = 30 s
Phase Ambiguity	Per Arc Bias	300 km	phase ambiguity resolution (Bertiger, et al. [14])
Geocenter Offset	Bias	3.0 cm	

Clock Post-Processing Used to Determine the Allan Deviation

The previous section showed how the GIPSY-OASIS was used to determine the DSAC clock offset x(t). However, for clock characterization it is more usual to work with the fractional frequency error y(t), the first derivative of x(t), which we will use in this section along with x(t). Also, in this section we will concentrate on the 2020 52-day run whose results first appeared in Burt, el al. [1] as this provides a very nice illustrative dataset.

The blue curve on the top plot of Figure 7 shows the y(t) produced from the processing described in the previous section for a day of data. A clear orbital period sinusoid is seen and this is primarily caused by the fact that the GPS processing measures DSAC clock x(t) in space and a reference atomic clock on the ground, typically one at the US Naval Observatory. Even if both of these clocks were perfect,
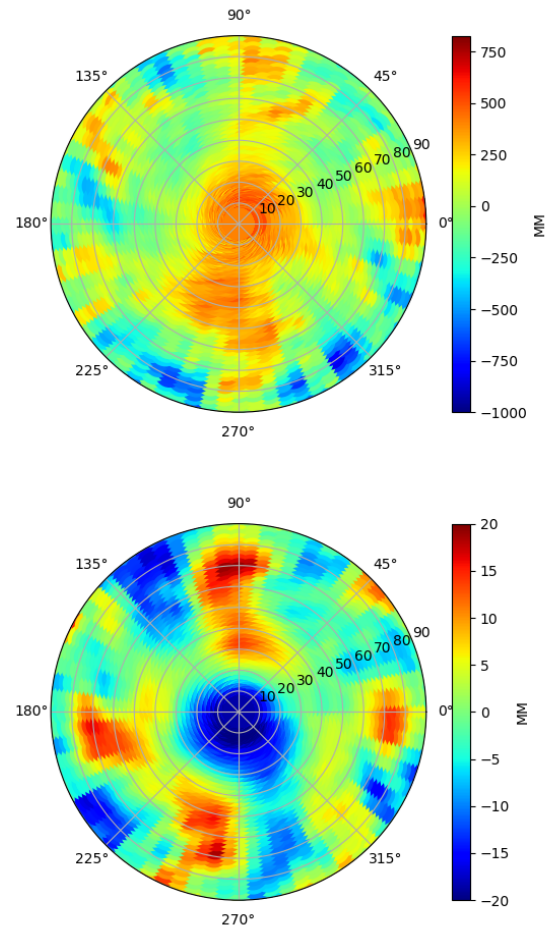

Figure 6: Multipath errors as PC (top) and LC (bottom) data fit residual maps.

the x(t) time difference between them would produce this sinusoidal y(t) oscillation, since these clocks are in different locations with different gravitational potentials and are also moving at different velocities resulting in clocks 'ticking' at different rates relative to one another (due to both the general relativistic gravitational redshift effect and the special relativistic transverse Doppler/time-dilation effect). Since the orbit determination process determines both the position **r** (and hence the gravitational potential) and the velocity **v** of the DSAC clock, we can and do apply a relativistic correction to the data, along with a GPS temperature calibration, that results in the magenta y(t) data shown in the top plot of Figure 7 and the associated Allan deviation, also shown in magenta, on the bottom plot. Note that the relativity correction we apply differs from the standard $-2\mathbf{r} \cdot \mathbf{v}/c^2$ correction to x(t) often applied to GPS satellite clocks that overcompensates for the effect of the J_2 potential term and, instead, we use the method described by Larson, et al. [15] that correctly corrects for the J_2 effect.

Figure 8 shows the Allan deviation of the full 2020 52-day Nature paper dataset [1]. In blue is the Allan deviation without any relativity correction or GPS temperature calibration that clearly shows relativistic effects dominate the
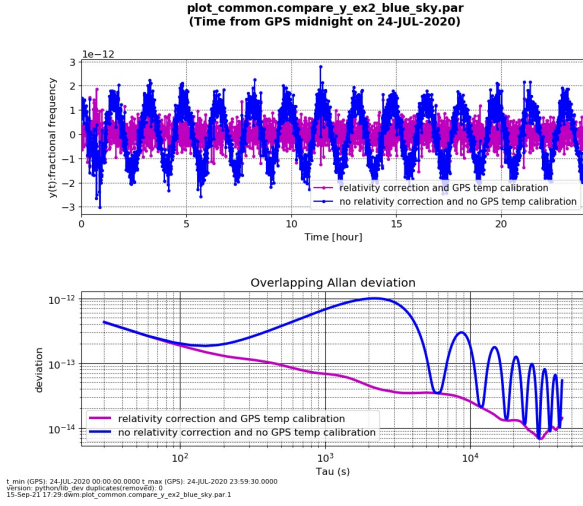
plot_common.compare_y_ex2_blue_sky.par
(Time from GPS midnight on 24-JUL-2020)

t_min (GPS): 24-JUL-2020 00:00:00.0000 t_max (GPS): 24-JUL-2020 23:59:30.0000
version: python/lib_dev duplicates(removed): 0
15-Sep-21 17:29:dwm:plot_common.compare_y_ex2_blue_sky.par:1

Figure 7: Top plot shows y(t) before relativity correction and GPS temperature calibration in blue and y(t) after relativity correction and GPS temperature calibration in magenta for a single day of data. A frequency bias has been removed from the y(t) data. Orbital variations primarily due to relativistic effects are clearly seen in the blue y(t) data. Bottom plot shows the corresponding Allan deviations which are the standard way to represent clock stability for different timescales Tau.

Allan Deviation on timescales past 100 s. However, when we correct for relativity, we get the red curve that also shows an orbital period Allan deviation signature but at a much lower level than produced by relativity. This phenomenon was predicted before launch. Testing of the GPS receiver showed that it produced an additional x(t) delay that depended on temperature where its largest effect is linear at approximately -130 psec/K (the full effect is calibrated using a quartic expression that also includes a temperature rate dependence). Since the OTB spacecraft at a height of about 720 km spends about 1/3 of each orbit in eclipse, the GPS receiver temperature also shows a sinusoidal temperature variation every orbit that consequently results in oscillatory x(t) variations resulting from the oscillatory temperature variations. After we apply the GPS temperature calibration to the relativity corrected data shown in the red curve of Figure 8, we then get the magenta curve in which both the relativity correction and GPS temperature calibration have been applied. It is this relativity corrected and GPS temperature calibrated y(t) data that can then be used to determine the Allan deviation of the DSAC clock on-orbit. One thing to note from Figure 8 is that the magenta y(t) data looks quite like the AD response of white frequency noise that conforms to $1/\sqrt{\tau}$, which is expected for a well-designed clock (see Section 5 for more details on the clock performance. It is also important to remember that the x(t) determined from the GPS receiver incorporates all effects along the signal chain from the clock to the GPS receiver, so effectively provides an upper limit on the actual clock performance because it includes systematic errors from all measurement system effects on top of the clock's actual performance.

plot_common.paper_relativity9b.par

start:23-JUL-2020 09:32:00.0000 stop:13-SEP-2020 18:14:00.0000
version: python/lib_dev duplicates(removed): 0
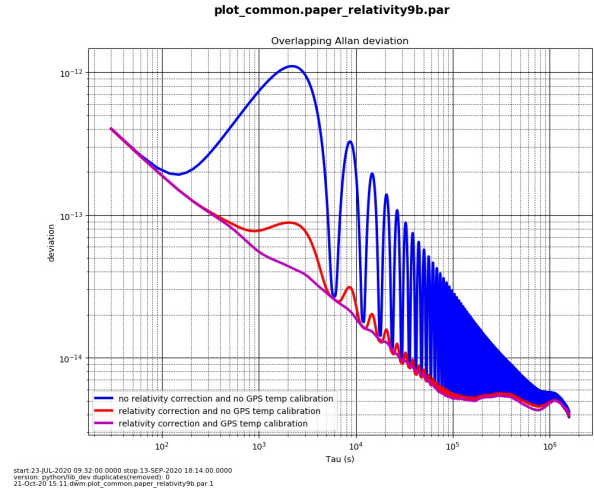21-Oct-20 15:11:dwm:plot_common.paper_relativity9b.par:1

Figure 8: Allan deviations for the 2020 52-day y(t) dataset at different stages of data calibration. Blue: no relativity correction or GPS temperature calibration bas been applied. Red: only relativity correction has been applied. Magenta: Both relativity correction and GPS temperature calibration have been applied. Note the 100 min orbital period (=T) relativistic effects produce the blue quasi-sinusoidal Allan deviation oscillations with a peak at tau=0.37*T and quasi-nulls at tau=n*T where n is a positive integer with an upper envelope that decreases as 1/tau. Thus, it is critical to remove relativity effects if you want to study the performance of an atomic clock in space.

The DSAC ion clock has been described in detail in Tjoelker, et al.[16] Many components of the DSAC clock design originated from prior developments described in Tjoelker, et al.[17] and Burt, et al. [18] and earlier physics package developments described in Prestage and Weaver [19] and Prestage, et al. [20] Here we summarize characteristics of the actual clock that was flown.

A block diagram for the DSAC system is shown in Figure 9. The basic components are the ion trap subsystem (includes the quadrupole and multi-pole ion traps and vacuum tube housing); the trap drive radio frequency electronics; the ultraviolet (UV) light subsystem (includes the UV light source, optics, and UV detection photo-multiplier tube (PMT)); the microwave/local oscillator (LO) subsystem (includes the USO); a tunable 40.5x GHz synthesizer to drive the mercury ion clock transition; a user output synthesizer; the FPGA-based clock controller, and the power system. The GPS receiver that was used to verify DSAC's long-term stability performance in-space is not shown in Figure 9.
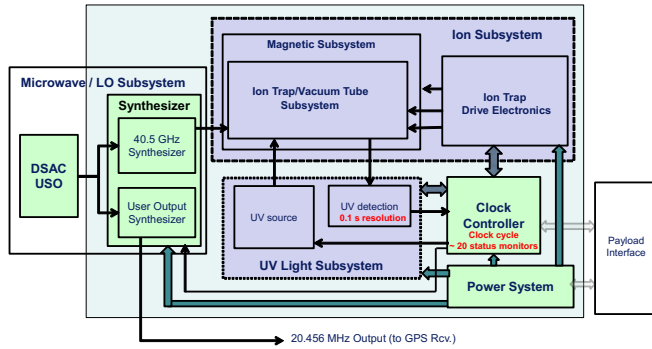
4. DSAC FLIGHT PERFORMANCE RESULTS

9

Figure 9: The DSAC system block diagram.

DSAC Systematic Sensitivities

Space clocks are subjected to a much harsher environment than laboratory clocks. For DSAC, the most important environmental sensitivities are magnetic and thermal variations. For instance, the magnetic field in one orbit can vary up to 250 milli-Gauss (for a polar Earth orbit) and can be 40 times greater than that in Jovian orbit [21]. Internal spacecraft temperatures may vary by several degrees over an Earth orbit. It is therefore critical to have accurate knowledge of the clock's environmental sensitivities so that the impact of variations in the environment can be determined. The DSAC clock consists of two ion traps: a quadrupole trap intended for ion loading, state preparation, and state detection, and a multipole trap designed for sensitive microwave interrogation of the clock transition. The multipole trap enables optimal long-term stability [11], but shortly before launch a depletion mechanism in the buffer gas used to cool ions was discovered. This mechanism is understood and will be corrected in future versions of the technology, but time and resources were not available to correct it in the DSAC instrument. Due to its much higher sensitivity to the buffer gas partial pressure, it was not feasible to continue operating the clock in the multipole trap. However, it was still possible to operate the clock in the quadrupole trap, though at a higher instability.

Sensitivity to variations in the number of ions trapped--As the number of trapped ions varies, associated changes in the trap volume occupied by the ions causes a change in the time-averaged trap rf seen by the ions. Ion motion driven by this rf field results in a second-order Doppler shift proportional to the velocity squared, which is therefore dependent on the number of ions trapped. While characterizing clock operation in space, this effect was measured by intentionally turning off ion loading so that the ion number changed significantly. In addition, while the ion number effect was changing monotonically, the temperature was not, so decoupling these two effects was straight forward. In the quadrupole trap a total clock fractional frequency shift due to the ion number effect of about -1×10^{-12} (from no ions to a full trap) was found to be consistent with measurements made with DSAC on the ground and with other trapped ion clocks operating in the quadrupole trap. A stability in ion number of 0.1% per day is required to reach a drift of $< 1\times10^{-15}$/day. After a prescribed

warmup time of about 1 week, the trapped ion number reached this level of stability while operating in space.

Temperature sensitivity—The DSAC DU does not have overall thermal control or insulation. Rather it depends on the low inherent thermal sensitivity of this technology and a long thermal time constant of the instrument. The overall temperature sensitivity of the clock is a combination of several effects, some that are not fundamental to the technology nor constant in time. For instance, thermally driven ion motion results in a second order Doppler shift (see Prestage, et al.[20]) is a fundamental effect, but thermally-induced changes in the magnetic field current, as well as temperature sensitivities of the USO, the GPS receiver, the synthesizers, and other electronics can in principle be engineered out. Furthermore, time-variations in temperature will lead to time-varying thermal gradients, which can result in measured variations in the effective temperature sensitivity for any macroscopic system [22].

Clock temperature sensitivity was measured in space with respect to temperature changes in the vacuum chamber of the clock. Since temperature variations of the vacuum chamber were smaller than the base plate, estimates of temperature sensitivity relative to the vacuum chamber can be considered a conservative worst case. The space craft experienced variations in temperature on several time scales. The corresponding peak-to-peak variation at the clock vacuum chamber was about 4 °C on an approximate 30 day period due to variations in the sun elevation above the orbital plane referred to as the beta angle (note that during this data set the space craft also executed two discrete orientation changes designed to keep the radiator pointing away from the sun – this interrupted the longer monthly variations giving the appearance of an approximate 15-day period), 0.5 °C with a daily period, and 0.3 °C with the orbital period of about 98 minutes. On the ground before launch an upper bound on the sensitivity magnitude in the quadrupole trap of 2×10^{-14}/°C was measured. A similar value was measured in space, but was found to vary over time to smaller values, often correlated with the beta angle, which changes the thermal gradient across the instrument. However, even a 2×10^{-14}/°C sensitivity only results in a 2×10^{-15} effect at the orbital period and $< 4\times10^{-15}$ at a day [23], both of which were below the measurement system noise floor in the Allan deviation.

Radiation effects—The clock was exposed to varying degrees of radiation depending on whether it passed through the South Atlantic Anomaly. These passes occurred several times each day as the spacecraft orbit precessed. The primary effects were changes in photo-multiplier tube (PMT) counts, and variations in the USO drift rate. Both effects are efficiently filtered out by the clock control loop [23] and do not significantly impact clock stability.

Magnetic—The DSAC DU magnetic subsystem consists of 3 mu-metal magnetic shields and a bias field coil. Two inner shields surround the vacuum tube (trap region) while a third outer shield forms an enclosure around the entire instrument (including most electronics). On the ground before launch,
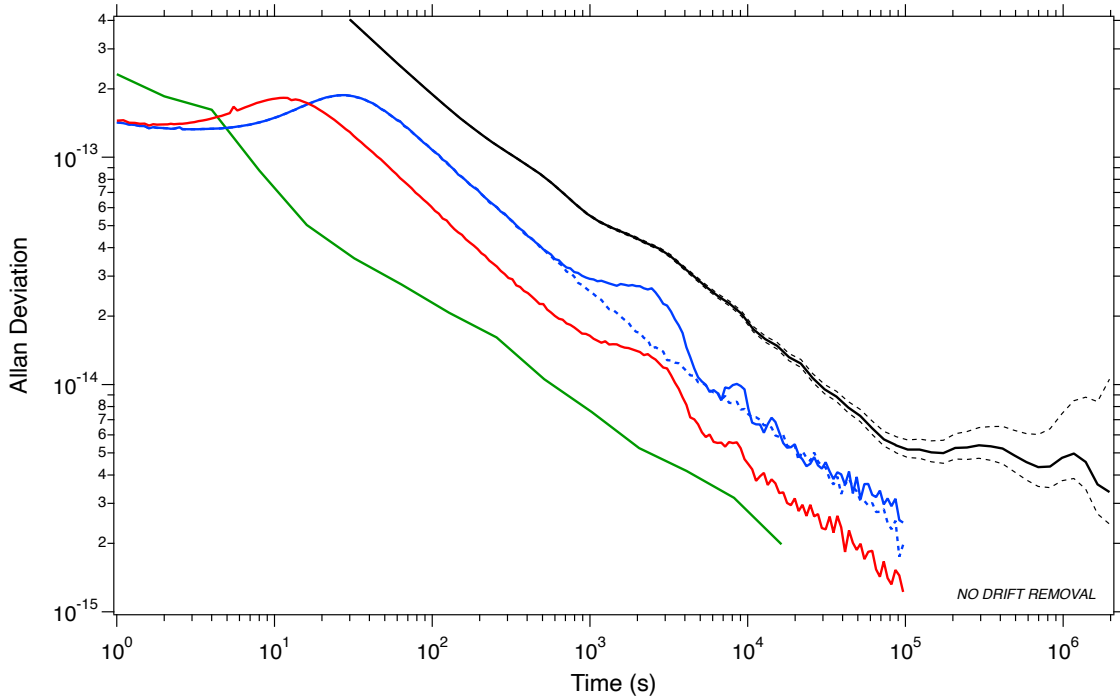
10

Figure 10: The Allan deviation of frequency offsets between the DSAC clock and the USNO master clock using GPS time transfer (solid black trace – the dashed black lines show 68% confidence intervals). In addition to clock noise, the data includes GPS system noise and is not drift-removed. The blue trace shows a simulation of clock performance including all known environmental perturbations, USO noise, aliasing, control loop effects, and ion clock signal noise, but not GPS noise (the dashed blue trace is the same with the environmental perturbations removed). The red trace shows the same simulation with more optimized clock parameters. For comparison, the green trace shows measured performance on the ground before the buffer gas depletion process was discovered. The black trace is an overlapping Allan deviation while all others are non-overlapping.

the magnetic sensitivity of the clock while operating in QP mode was measured to be a maximum of 7×10^{-14}/Gauss (depending on the direction of the field). The orbital external magnetic field variation of approximately 0.25 gauss peak-to-peak resulted in a worst-case $0.36 \times 0.25 \times 7 \times 10^{-14} = 6 \times 10^{-15}$ contribution to the Allan deviation at an averaging time of 0.37×98 minutes or about 2200 seconds [23], below the noise floor for that averaging time.

Other Systematic Effects—The other primary systematic effects of this technology are decoupled, to first order, from the environment and are smaller than the thermal and magnetic effects. They have been well characterized elsewhere (Burt, et al.[24]) and remain the same or similar for the DSAC clock. The largest of these are caused by variations in the partial pressure of background gases (see Chung, et al.[25] and Yi, et al.[26]). Drift due to background gas evolution was estimated to be $< 5\times10^{-16}$/day.

Results for DSAC Operation in Space

Clock Performance—Figure 10 shows the Allan deviation of the clock during a long run of over 50 days (see the "Clock Post-Processing Used to Determine the Allan Deviation" section in this paper for details on how this Allan deviation is derived). The measurement consists of a comparison between the DSAC clock and the USNO master clock using GPS time transfer. This measurement includes GPS system noise and

has no drift removed. In the short-term up to averaging times of about 1 day, the Allan deviation is measurement-system limited. For long time scales, a fit of the frequency offsets to a straight line gives an estimate of $+3.0(0.7)\times10^{-16}$/day drift, consistent with the measured Allan deviation, which remains in the low 10^{-15} range past 10^6 seconds [1]. This is a key result of this work and demonstrates this technology's suitability to applications requiring autonomous operation. It is important to note that this result was also obtained in the presence of a 9 °C variation in the temperature of the baseplate with no active temperature control, and 250 milli-Gauss orbital variations in the magnetic field, thereby demonstrating this technology's robustness in the presence of significant environmental perturbations. Subsequent runs of similar length produced similar long-term performance showing that this is a reliable feature of this clock. In the first subsequent long run, the number of ions was out of equilibrium for the first 3 weeks. When this part of the data is excluded, the long-term drift is $-5.4(4.4)\times10^{-16}$/day (the larger uncertainty due to the shorter net time period). For the second additional run, completed on September 18, 2021, the ion number was more stable throughout and a simple fit to a straight line with no data removed gives a drift of $-5.8(0.7)\times10^{-16}$/day.

Clock Lifetime—While the DSAC mission requirement was only 2 years, future applications of this technology require longer instrument life. The key parts of the clock that limit

this lifetime are the UV light source ("lamp") and background gas evolution with the latter including the buffer gas neon, mercury vapor used to load the trap, and other background gasses that can cause decoherence in the clock signal. The lifetime for the current DSAC clock is found to be in excess of 4 years, limited by the lamp. The other sources place a limit of 7 years or more. The type of lamp used has previously demonstrated a 3–5-year life. At the end of the mission, the lamp used on DSAC had 4 years of operation and showed only a slight degradation in performance as indicated by optical pumping time and clock signal size. Work is under way to improve the lifetime of UV lamps past 5 years. As mentioned earlier, the shuttling process that moves ions from one trap to another is sensitive to neon pressure. Measurements were taken on the ground to calibrate the pressure to the number of consecutive round-trip shuttles that can be performed so that the number of shuttles could serve as a proxy for a pressure gauge. Periodic measurements were made and it was determined that while the neon pressure continued to decay slowly, the rate would still support quadrupole trap operation for more than 9 years. The trap loading rate is proportional to the level of background neutral mercury vapor present. In space we monitored the 1/e load time and found that it would not limit clock operation for at least 7 years. Finally, increasing levels of background gas can lead to decoherence in the clock signal via collisions. These collisions will manifest themselves as a limit on the clock interrogation time and/or a broadening of the clock transition spectral line. A degradation in neither of these was observed in space leading to the conclusion that such gas evolution is not clock life limiting.

5. DEEP SPACE ANALOG ORBIT DETERMINATION EXPERIMENT

The deep-space navigation analog experiment utilized the flight GPS tracking data to demonstrate orbit determination performance using one-way and pseudo-two-way GPS Doppler data with measurement quality, quantity, and schedule characteristics (such as tracking data density, duration, and geometric variability) that are operationally similar to that available in deep-space navigation. Evaluation of clock performance in low-Earth orbit required the use of high-fidelity models of the orbital dynamics and GPS measurements and the characterization of expected modeling errors [27].

Careful selection of GPS data, artificial data degradation, and appropriate data weighting allowed for a demonstration of orbit determination that is analogous to that of a Mars orbiter such as the Mars Reconnaissance Orbiter (MRO). The flight data selected for the results presented here spans 30-SEP-2019 00:00:00 GPS through 02-OCT-2019 00:00:00 GPS. (A 48-hour data span is typical for MRO orbit reconstruction.) For MRO operations, orbit overlaps on the order of 12 hours are used for assessment of solution consistency; for the navigation analog experiment, the orbit solution can be compared directly to that estimated using the full set of GPS carrier phase and pseudo-range tracking data

and the highest-fidelity models available. This orbit solution is referred to as the "truth" solution.

Methodology

The navigation analog experiment used the following methodology:

1. Estimate "truth" OTB orbit and DSAC clock using full set of GPS carrier phase and pseudo-range data

2. Degrade GPS carrier phase and pseudo-range data with simulated media errors

3. Downselect degraded GPS carrier phase data to represent DSN tracking of a Mars orbiter

4. Convert downselected GPS carrier phase data to GPS Doppler data

5. Degrade Earth fixed frame model with simulated Earth orientation parameter errors

6. Process GPS Doppler data with navigation filter

7. Compare converged orbit solution to "truth" orbit

For this overview presentation a brief qualitative review of these steps is now described, for a more thorough overview see Seubert, et. al. [28].

Data Degradation—The DSAC GPS receiver collects dual frequency (L1 and L2) carrier phase and pseudo-range tracking data, which is linearly combined to remove first-order ionospheric errors from the tracking data. Furthermore, at an altitude of 720 km the spacecraft is well above the troposphere. Tracking data with no media effects (to first order) is desired for optimal clock and orbit estimation, but is not realistically representative of the quality of radiometric tracking data collected to support deep space navigation. In reality, radiometric tracking signals passing between the Deep Space Network (DSN) ground stations and the spacecraft they support must traverse both the troposphere, ionosphere, and solar plasma. Dual-frequency tracking to remove first-order ionospheric and solar plasma errors is not standard practice. Though tropospheric and ionospheric calibrations are routinely used for ground-based navigation, the calibrations include residual errors that cannot be removed from the raw tracking data. To account for these effects, simulated media delays representing the residual error remaining after applying empirical media calibrations were applied to the data at levels that would be consistent with the expected calibration errors.

Data Downselection—Tracking data of an Earth orbiting satellite from the full GPS constellation provides a rich geometric diversity in a short period of time; GPS signals as observed by the spacecraft receiver rise and set in a matter of minutes, originate from six unique orbital planes, and (for the OTB spacecraft) track on average nine satellites at one time. In contrast, DSN tracking of a spacecraft in deep space suffers severely limited geometric variation. For example, DSN tracking signals as observed by a Mars orbiter such as MRO appear to originate from a relatively fixed inertial point
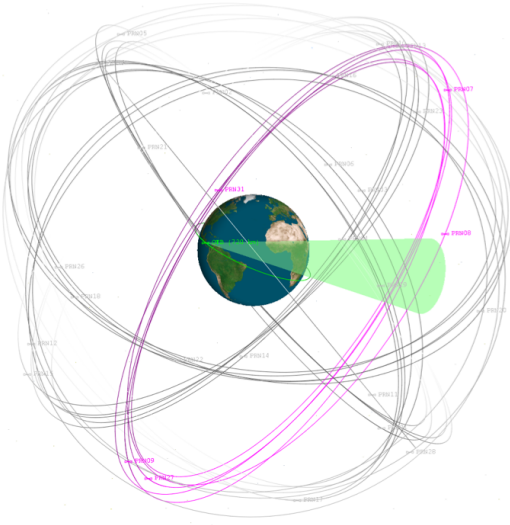
Figure 11: GPS tracking data selection to better represent DSN tracking of a low-altitude Mars orbiter. The observability cone half-angle was chosen arbitrarily for illustrative purposes

over a span of a few days; the signals originate from approximately a single orbital plane and primarily from a single ground station at a time. Furthermore, GPS tracking of an Earth orbiter is continuous, whereas DSN tracking of a Mars orbiter includes lengthy (8–10 hour) tracking gaps when the DSN is committed to tracking another spacecraft.

To better represent the limited duration, density and geometric variability of DSN tracking, GPS tracking data is carefully downselected to a more limited data set. As shown in Figure 11, GPS tracking data is constrained to originate from a single GPS orbital plane designation (for the present data the 'B' plane), and within a small angular constraint of the GPS orbit ascending node crossing. The angular constraint is defined as the amount of DSN ground station angular rotation seen by a low-altitude Mars orbiter over one orbit, denoted by ω in Figure 12. Assuming a Martian circular orbit with a period of 100 minutes, which must be noted is commensurate with OTB's orbit but is not physically possible for a Martian satellite, the worst-case DSN visibility will result in approximately 50 minutes of tracking per orbit. This bounding case results in a DSN subtended angle of 12.5°; as such, the GPS tracking data is constrained to originate from within ±6.25° of the ascending node crossing.

Using the geometry constraints discussed, we downselected the full GPS carrier phase and pseudo-range tracking data set to a much-reduced data set as illustrated by the Doppler postfit residuals in Figure 13. The reduction leaves approximately 0.2% of the original data for utility in the navigation analog experiment.

GPS Doppler Measurements—The downselected GPS carrier phase measurements are converted into Doppler space to reflect current DSN radiometric tracking. This conversion is performed by differencing the degraded (e.g., media corrupted) phase measurements $\phi(t)$ and averaging over the
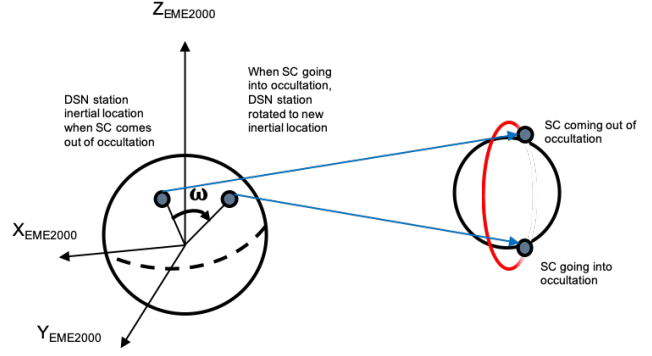

Figure 12: Per-orbit DSN angular rotation as seen by a low-altitude Mars orbiter.

integration time T. The average differenced phase is then converted from velocity space to frequency space via scaling by the ratio of the GPS signal frequency f_{LC} (a linear combination of L1 and L2 frequencies) to the speed of light c as follows

$$\Delta f\left(t - \frac{T}{2}\right) = \frac{f_{LC}}{cT}\left(\phi(t) - \phi(t-T)\right).$$

A Doppler integration time of 60 seconds, typical for Mars orbiter trajectory reconstruction, was utilized.

The GPS phase measurements include both transmitter and receiver clock error according to

$$\phi(t) = \left(\rho(t) + \delta t_r(t) - \delta t_t\big(t - \rho(t)\big)\right)c,$$

where ρ is the signal transit light time, δt_r is the receiver clock error, and δt_t is the transmitter (GPS) clock error. By applying the JPL Analysis Center GPS clock solutions, the transmitter clock errors are reduced to a level below the phase measurement noise.

In contrast, the receiver clock errors are entirely manifested in one-way GPS Doppler as

$$\phi_{F1}(t) = \Big(\rho(t) + \delta t_r(t) - \delta t_t\big(t - \rho(t)\big) \\ + \delta t_t^*\big(t - \rho(t)\big)\Big)c \approx \big(\rho(t) + \delta t_r(t)\big)c.$$

Therefore, the one-way GPS Doppler is directly analogous to uplink one-way DSN Doppler, in which the DSN transmitter clock error is negligible but the onboard clock error still contributes to the measurement.

As GPS is a transmit-only navigation system, it is not possible to collect true two-way measurements; therefore, one-way GPS Doppler data must be manipulated to serve as a surrogate for true two-way Doppler data. Two-way Doppler data differs from one-way Doppler data in several significant ways. For two-way DSN data transmitted and received at DSN ground antennas, the onboard clock error does not contribute to the measurement. Because the two-way measurements are derived from the round-trip light time—not the one-way light time—the measurement sensitivity to
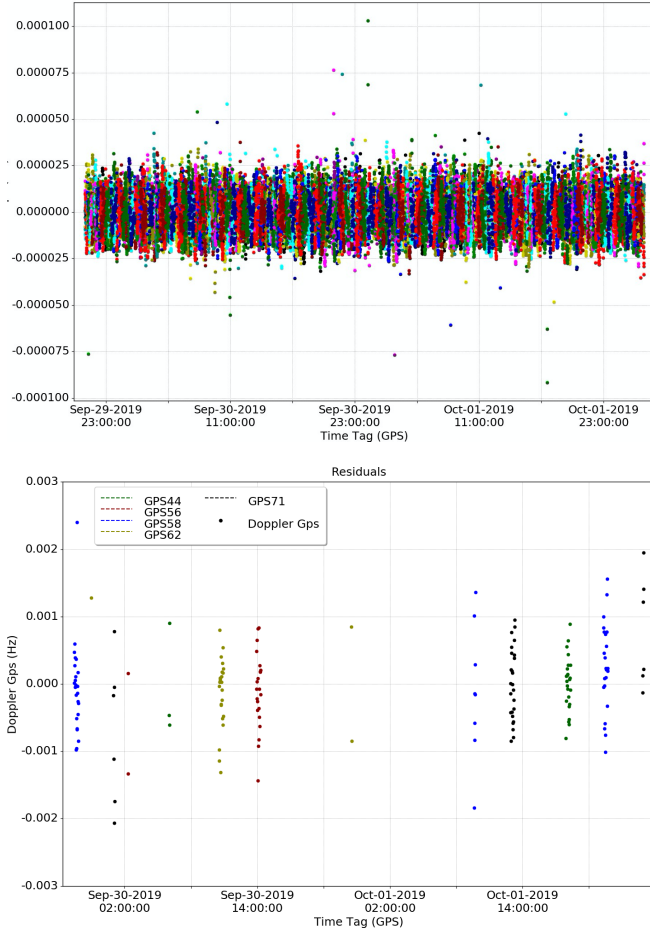
Figure 13: (Top) GPS carrier phase postfit residuals for full GPS tracking. (Bottom) Downselected GPS Doppler postfit residuals (pseudo-two-way Doppler). Colors denote GPS transmitters.

the estimated dynamic state is scaled by a factor of 2. Finally, for frequencies such as S- and X-band, where the radiometric signal noise is dominated by uncorrelated path-dependent effects, two-way measurements are a factor of $\sqrt{2}$ noisier than one-way measurements. The combined effect of increased measurement noise and increased measurement sensitivity can be handled by scaling the nominal one-way data weight by a factor of $\sqrt{2}$. The onboard clock error can be removed or reduced via calibration, which leads to the concept of pseudo-two-way GPS Doppler.

In simulation analyses, the true onboard clock error is known and, therefore, can be entirely removed from the one-way GPS Doppler measurements. This measurement is now directly analogous to two-way DSN Doppler data, in which the clock errors are not the dominant measurement error source. In actual flight, however, the true onboard clock error is unknown and, therefore, cannot be removed from the one-way GPS Doppler data via calibration. As a proxy, the estimated onboard ("truth") clock solution can be removed from the one-way GPS phase data to create pseudo-two-way GPS phase measurements $\phi_{pF2}(t)$ in which only the residual clock error remains:

$$\phi_{pF2}(t) = \left(\rho(t) + \delta t_r(t) - \delta t_t\left(t - \rho(t)\right) - \delta t_r^*(t) \right.$$
$$\left. + \delta t_t^*\left(t - \rho(t)\right)\right)c \approx \rho(t)c.$$

Although both data types are physically one-way measurements, comparisons of navigation performance using one-way GPS Doppler and pseudo-two-way GPS Doppler provides insight into the navigation performance that could be expected if true two-way tracking data were possible.

The one-way GPS Doppler data weight is determined by converting 1 cm of phase noise to the Doppler domain, resulting in a data noise of approximately 2.204 mHz (0.23 mm/s). Scaling by $1/\sqrt{2}$, the pseudo-two-way GPS Doppler data weight is approximately 1.558 mHz (0.08 mm/s).

Earth Orientation Model Degradation—Deep-space navigation must also contend with errors in the modeled orientation of the Earth-fixed reference frame relative to the inertial reference frame, either estimating or considering errors in the Earth's pole orientation and the Universal Time 1 (UT1) time frame [29]. Errors in the fixed-frame pointing of the Earth's pole, assuming the *z* direction is aligned with the pole, and UT1 time frame were simulated at levels that are consistent with those for typical DSN data and applied to the navigation analog filter's nominal Earth fixed frame, thus degrading the nominal model to better reflect typical deep space navigation.

Navigation Filter—The navigation analog upper-diagonal sequential Kalman filter configuration is shown in Table 4. In addition to the initial spacecraft position and velocity states, the filter states include corrections to several dynamic modeling errors. A bias correction to the drag coefficient and a constant scale factor on the solar pressure are estimated to account for mismodeling of the spacecraft bus and solar flux activity. Additional states compensate for observed empirical acceleration mismodeling, which is dominant in the orbital normal direction. It is theorized that this observed spacecraft acceleration is due to reradiation thermal effects, as the acceleration is aligned with the spacecraft radiator.

Table 4: Navigation filter configuration

Estimated Parameter	Parameter Type	A Priori Uncertainty (1σ)
Position (EME2000)	Dynamic	10 m
Velocity (EME2000)	Dynamic	1 cm/s
OTB drag coefficient	Bias	0.25 (10%)
OTB solar pressure scale factor	Bias	0.1 (10%)
Orbital accel. coefficients	Bias	10 pm/s^2

Empirical accel., radial	Stochastic ECRV, $\tau = 600$ s, Batch = 60 s	2 pm/s^2
Empirical accel., tangential	Stochastic ECRV, $\tau = 600$ s, Batch = 60 s	10 pm/s^2
Empirical accel., normal	Stochastic ECRV, $\tau = 600$ s, Batch = 60 s	15 pm/s^2
Clock drift (one-way GPS Doppler only)	Stochastic White Batch = 9 hours	1×10^{-9}

The filter has been empirically tuned to estimate an orbital acceleration in the normal direction, as well as stochastic accelerations in the spacecraft-fixed reference frame:

$$a_N(t) = A \, sin\left(2\pi \frac{t - t_0}{P}\right) + B \, cos\left(2\pi \frac{t - t_0}{P}\right),$$

where P denotes orbital period and t_0 is the initial epoch. The filter includes only one accommodation for the one-way data processing, which is to add a clock drift estimate every nine hours (approximating DSN station acquisition for a Mars orbiter). This is necessary because of small frequency offsets that would exist between transmitting and receiving hardware.

Orbit Determination Performance

The navigation analog experiment was conducted using both one-way and pseudo-two-way GPS Doppler measurements, enabling a direct investigation into the effect of the onboard clock stochastic behavior on orbit reconstruction. As described in the following section, a calibration of the onboard clock deterministic time offset and rate must be performed for optimal orbit reconstruction when only using Doppler data. All results presented here represent the smoothed results of a converged upper-diagonal sequential Kalman filter.

As will be shown, both the tangential and normal components of the covariance matrix are significant; hence it is necessary to decompose the covariance matrix into its principal directional components for a meaningful computation of the three-dimensional uncertainty. Following eigenvalue decomposition, the root sum square (RSS) of the covariance matrix diagonal values is computed; we refer to this three-dimensional uncertainty representation as σ_{RSS}.

Pseudo-two-way GPS Doppler—The postfit pseudo-two-way GPS Doppler measurement residuals Figure 13 shown in demonstrate that the filter is able to fit the data very well. The data residuals are Gaussian with a root mean square well below the assigned data noise of 1.558 mHz, which indicates that the data weight (based off a 1 cm GPS carrier phase noise level) is conservative, as expected.

Figure 14 presents the differences between the navigation analog orbit solution and the "truth" orbit solution determined using the full GPS constellation. The three-dimensional $3\sigma_{RSS}$ is 4.452 m in position and 3.969 mm/s in velocity (not shown). These results are in family with the operational orbit reconstruction performance of MRO.
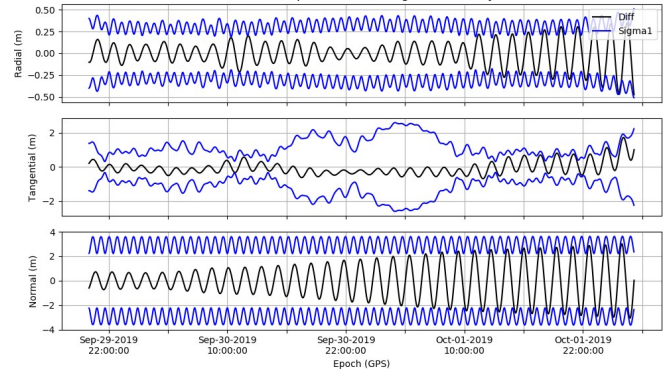

Figure 14: Orbit errors and 3σ uncertainty envelope (pseudo-two-way Doppler). The 3σ formal uncertainty bounds shown in blue correspond to the navigation analog solution. These orbit errors are presented in the spacecraft-fixed radial, tangential, and orbit normal reference frame. The uncertainty inflation—primarily visible in the tangential direction, but observed to a lesser degree in the radial direction as well—is due to the lengthy tracking data gaps over approximately 30-SEP-2019 14:00 GPS through 30-SEP-2019 22:30 GPS (8.4 hours) and 30-SEP-2019 22:30 GPS through 01-OCT-2019 09:30 GPS (11 hours).

The pseudo-two-way GPS Doppler results demonstrate that the estimated onboard clock solution can be effectively removed from the data, such that orbit reconstruction based on GPS Doppler can be performed at a level commensurate with current low-altitude Mars orbiters. These results establish a baseline against which one-way GPS Doppler performance can be compared.

One-Way GPS Doppler with Clock Calibration—As discussed, the primary differences between pseudo-two-way and one-way GPS Doppler are appropriate two-way data weighting, an additional filter state to estimate an onboard clock rate every 9 hours, and the full inclusion of the onboard clock's deterministic and stochastic. Additionally, when only processing Doppler data, there is a need to account for an initial clock bias because the navigation analog filter has no means to deal with it. The solution to eliminate a clock bias's effect on the navigation solution is to either include range data in the processing, or perform a calibration of the deterministic onboard clock bias and clock rate errors. It is straightforward to calibrate for deterministic clock effects using pseudo-range data and/or process it along with the one-way Doppler data, as range measurements possess strong observability of onboard clock bias effects. The combination of Doppler and two-way range data is routinely collected during typical deep space navigation operations; however, one-way range data is not a service that is yet provided by the DSN. To fully realize the benefit of one-way radio tracking for deep space navigation will require the addition of DSN one-way range data tracking.

For the current processing, the deterministic clock calibration was performed by processing 24 hours of the downselected one-way GPS Doppler data and corresponding pseudo-range
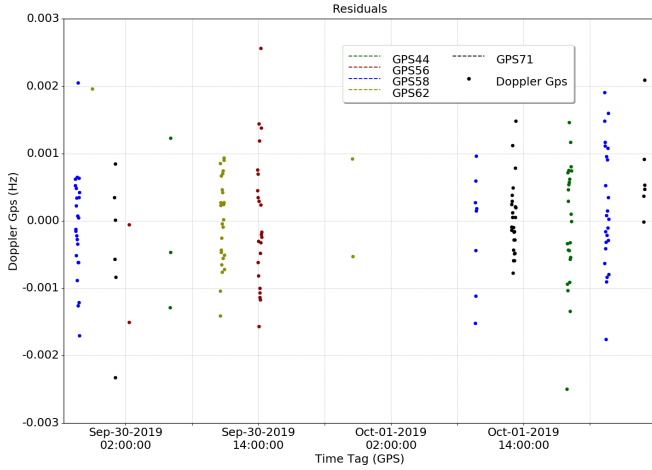
Figure 15: GPS Doppler postfit residuals (one-way Doppler with clock calibration).

Figure 16: Orbit errors and 3σ uncertainty envelope for one-way Doppler with clock calibration.

data with a filter focused on the clock solution, doing so yielded 0.795215 ms ±2 ns (1σ) and 1.6 pHz/Hz ±1.0 pHz/Hz for the initial clock bias and rate, respectively.

The one-way GPS Doppler analysis was then initialized using these estimated bias and rate values (an alternative approach would have been to include pseudo-range in the estimation process). The stochastic onboard clock errors were not accounted for in any way, aside from the filter's estimation of a stochastic clock rate every 9 hours. The effect of the deterministic clock calibration is shown in Figure 15 and Figure 16. Compared to the two-way reduced dataset residuals in Figure 13, there is no obvious change to the postfit residuals, illustrating not only that the filter is able to fit the data quite well, but also that the deterministic clock bias and rate are virtually undetectable to the orbit analyst inspecting the data residuals. The 3σ$_{RSS}$ is 8.229 m in position and 6.591 mm/per in velocity; the inflation relative to the pseudo-two-way 3σ$_{RSS}$ is due to the stochastic clock rate filter state but still in family with current low-altitude Mars orbit reconstruction.

The results of the DSAC deep-space navigation analog experiment demonstrate that DSAC may be utilized as a deep space navigation instrument and that for applications requiring the most demanding accuracy, a calibration step of the deterministic onboard clock offset and clock rate would be necessary to achieve those requirements. The one-way GPS Doppler and pseudo-two-way GPS Doppler solutions—both less than 10 m 3-σ formal uncertainty—are in family with current low-altitude Mars orbit reconstruction performance, and prove that one-way radiometric data can provide orbit solutions that are on par with the traditionally-utilized two-way tracking data. Furthermore, the entire navigation analog experiment was performed using the Monte navigation software currently used for deep- space navigation. By carefully considering modeling effects and data processing, this experiment also demonstrated the ability to perform a proxy navigation experiment using GPS tracking data of an Earth orbiter in lieu of demonstrating the DSAC payload directly in the Mars environment.
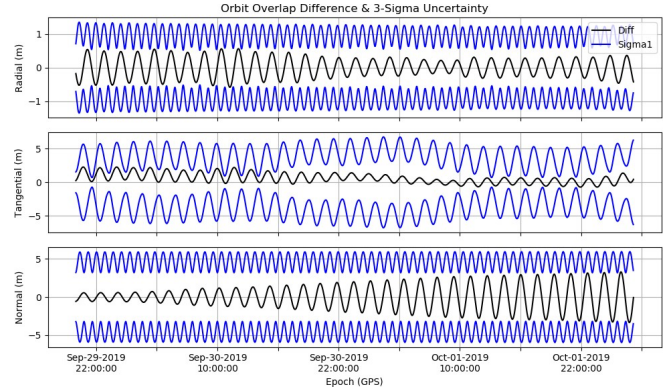
6. DSAC-2

DSAC's successes have warranted development of a next generation DSAC, called DSAC-2, that will be hosted on NASA's VERITAS mission to Venus. DSAC-2 intends to be smaller, use less power, and be longer-lived than DSAC-1 while maintaining excellent performance. Lessons learned, which have been thoroughly documented in DSAC-1's Technology Advancement Report, will be applied to the design and development of DSAC-2. This will facilitate the addition of DSAC-2's desired improvements, as well as, aiding in developing and easier to manufacture design; hence making it ready for future NASA, DoD, or commercial applications. Current plans are for VERITAS to launch later in the decade and, for the first two years after launch, to operate DSAC-2 and demonstrate its utility for deep space navigation and radio science as part of the DSAC-2 Technology Demonstration Opportunity (TDO). The DSAC-2 TDO is supported by NASA's Science Mission Directorate and Space Technology Mission Directorate as means to demonstrate and infuse this promising technology.

7. CONCLUSION

The DSAC mission operated for over two years and completed its mission on September 18, 2021. DSAC performed at levels well beyond expectations and has proven to be a robust space atomic clock. The clock exceeded all stability expectations with a stability (including drift) at a day of ~ 3×10^{-15} and a long-term linear frequency drift below 3×10^{-16}/day. Furthermore, its sensitivities to environmental effects, such as temperature and magnetic fields, were minimal. In the context of an analog deep space navigation experiment, the one-way radiometric tracking derived using the clock proved to be sufficient for orbit determination at performance levels similar to its two-way counterpart; validating its future use for navigation.

16

REFERENCES

[1] E. A. Burt *et al.*, "Demonstration of a trapped-ion atomic clock in space," *Nature*, vol. 595, no. 7865, pp. 43–47, 2021, doi: 10.1038/s41586-021-03571-7.

[2] T. A. Ely, J. Seubert, and J. Bell, "Advancing Navigation, Timing, and Science with the Deep-Space Atomic Clock," in *Space Operations: Innovations, Inventions, and Discoveries*, American Institute of Aeronautics and Astronautics, Inc., 2015, pp. 105–138. doi: 10.2514/5.9781624101991.0105.0138.

[3] T. A. Ely, E. A. Burt, J. D. Prestage, J. M. Seubert, and R. L. Tjoelker, "Using the Deep Space Atomic Clock for Navigation and Science," *IEEE Transactions on Ultrasonics, Ferroelectrics, and Frequency Control*, vol. 65, no. 6, pp. 950–961, Jun. 2018, doi: 10.1109/TUFFC.2018.2808269.

[4] T. A. Ely, J. Seubert, N. Bradley, T. Drain, and S. Bhaskaran, "Radiometric Autonomous Navigation Fused with Optical for Deep Space Exploration," *The Journal of the Astronautical Sciences*, vol. 68, no. 1, pp. 300–325, 2021, doi: 10.1007/s40295-020-00244-x.

[5] F. de Marchi and G. Cascioli, "Testing general relativity in the solar system: present and future perspectives," *Classical and Quantum Gravity*, vol. 37, no. 9, p. 95007, Apr. 2020, doi: 10.1088/1361-6382/ab6ae0.

[6] S. Desai, "GIPSY-OASIS." https://gipsy-oasis.jpl.nasa.gov/

[7] S. Flanagen and T. A. Ely, "Navigation and Mission Analysis Software for the Next Generation of JPL Missions," 2001.

[8] J. Seubert and T. Ely, "Deep Space Atomic Clock technology demonstration mission onboard navigation analog experiment," in *Advances in the Astronautical Sciences*, 2016, vol. 158.

[9] S. C. Wu, T. P. Yunck, and C. L. Thornton, "Reduced-dynamic technique for precise orbit determination of low earth satellites," *Journal of Guidance, Control, and Dynamics*, vol. 14, no. 1, 1991, doi: 10.2514/3.20600.

[10] W. Bertiger *et al.*, "Sub-Centimeter Precision Orbit Determination with GPS for Ocean Altimetry," *Marine Geodesy*, vol. 33, 2010, doi: 10.1080/01490419.2010.487800.

[11] J. M. Dow, R. E. Neilan, and C. Rizos, "The International GNSS Service in a changing landscape of Global Navigation Satellite Systems," *Journal of Geodesy*, vol. 83, no. 3–4. 2009. doi: 10.1007/s00190-008-0300-3.

[12] Förste, C. *et al.*, "A new release of EIGEN-6: The latest combined global gravity field model including LAGEOS, GRACE and GOCE data from the collaboration of GFZ Potsdam and GRGS Toulouse," *EGU General Assembly 2012*, vol. 14, 2012.

[13] D. Kuang, W. Bertiger, S. D. Desai, B. J. Haines, and D. N. Yuan, "Observed geocenter motion from precise orbit determination of GRACE satellites using GPS tracking and accelerometer data," *Journal of Geodesy*, vol. 93, no. 10, 2019, doi: 10.1007/s00190-019-01283-5.

[14] W. Bertiger *et al.*, "Single receiver phase ambiguity resolution with GPS data," *Journal of Geodesy*, vol. 84, no. 5, 2010, doi: 10.1007/s00190-010-0371-9.

[15] K. M. Larson, N. Ashby, C. Hackman, and W. Bertiger, "An assessment of relativistic effects for low Earth orbiters: The GRACE satellites," *Metrologia*, vol. 44, no. 6, 2007, doi: 10.1088/0026-1394/44/6/007.

[16] R. L. Tjoelker *et al.*, "Mercury Ion Clock for a NASA Technology Demonstration Mission," *IEEE Transactions on Ultrasonics, Ferroelectrics, and Frequency Control*, vol. 63, no. 7, 2016, doi: 10.1109/TUFFC.2016.2543738.

[17] R. L. Tjoelker *et al.*, "Mercury Atomic Frequency Standards for Space Based Navigation and Timekeeping," in *Proceedings of the 43rd Annual Precise Time and Time Interval Systems and Applications Meeting*, 2011, pp. 293–304.

[18] E. A. Burt, B. Tucker, K. Larsen, R. Hamell, J. Prestage, and R. Tjoelker, "Next Generation JPL Ultra-stable Trapped Ion Atomic Clocks," in *Proceedings of the 45th Annual Precise Time and Time Interval Systems and Applications Meeting*, Dec. 2013, pp. 55–61.

[19] J. D. Prestage and G. L. Weaver, "Atomic Clocks and Oscillators for Deep-Space Navigation and Radio Science," *Proceedings of the IEEE*, vol. 95, no. 11, pp. 2235–2247, Nov. 2007, doi: 10.1109/JPROC.2007.905130.

[20] J. D. Prestage, Meirong Tu, S. K. Chung, and P. MacNeal, "Compact microwave mercury ion clock for space applications," in *2008 IEEE International Frequency Control Symposium*, May 2008, pp. 651–654. doi: 10.1109/FREQ.2008.4623080.

[21] C. A. Jones, "A dynamo model of Jupiter's magnetic field," *Icarus*, vol. 241, pp. 148–159, Oct. 2014, doi: 10.1016/J.ICARUS.2014.06.020.

[22] B. Jaduszliwer, N. Bhaskar, and N. Russo, "Observation of thermal hysteresis in atomic clocks, and its impact on timekeeping," in *Proceedings of the Annual IEEE International Frequency Control Symposium*, 1997, pp. 270–272. doi: 10.1109/freq.1997.638558.

[23] D. G. Enzer, W. A. Diener, D. W. Murphy, S. R. Rao, and R. L. Tjoelker, "Drifts and Environmental Disturbances in Atomic Clock Subsystems: Quantifying Local Oscillator, Control Loop, and Ion Resonance Interactions," *IEEE Transactions on Ultrasonics, Ferroelectrics, and Frequency Control*, vol. 64, no. 3, pp. 623–633, Mar. 2017, doi: 10.1109/TUFFC.2016.2636088.

[24] E. A. Burt, S. Taghavi, J. D. Prestage, and R. L. Tjoelker, "Stability evaluation of systematic effects in a compensated multi-pole mercury trapped ion frequency standard," in *2008 IEEE International Frequency Control Symposium*, May 2008, pp. 371–

376. doi: 10.1109/FREQ.2008.4623022.

[25] S. K. Chung, J. D. Prestage, R. L. Tjoelker, and L. Maleki, "Buffer gas experiments in mercury (Hg+) ion clock," in *Proceedings of the 2004 IEEE International Frequency Control Symposium and Exposition, 2004.*, 2004, pp. 130–133. doi: 10.1109/FREQ.2004.1418441.

[26] L. Yi, S. Taghavi-Larigani, E. A. Burt, and R. L. Tjoelker, "Progress towards a dual-isotope trapped mercury ion atomic clock: Further studies of background gas collision shifts," in *2012 IEEE International Frequency Control Symposium Proceedings*, May 2012, pp. 1–5. doi: 10.1109/FCS.2012.6243693.

[27] T. A. Ely, D. Murphy, J. Seubert, J. Bell, and D. Kuang, "Expected Performance of the Deep Space Atomic Clock Mission," 2014.

[28] J. Seubert, T. Ely, and J. Stuart, "Results of the Deep Space Atomic Clock Deep Space Navigation Analog Experiment," in *Advances in the Astronautical Sciences, Vol. 175*, Aug. 2020, pp. 2965–2980.

[29] T. D. Moyer, *Formulation for Observed and Computed Values of Deep Space Network Data Types for Navigation*. Hoboken, N.J.: Wiley-Interscience, 2003.

BIOGRAPHIES

Dr. Todd Ely received a B.S. in Aeronautical and Astronautical Engineering in 1986, a M.S. and Ph.D. in Aeronautics and Astronautics in 1988 and 1996, respectively, from Purdue University. Since 1999, he has been at the Jet Propulsion Laboratory developing and implementing navigation systems and architectures for many projects - big and small – including the Mars Network, the Electra radio, JPL's MONTE navigation software, the Constellation Program and the Altair lunar lander. Since 2011, he has been the principal investigator for the DSAC Technology Demonstration Mission that completed operations in September 2021. Currently, he is the DSAC-2 Technology Demonstration Investigation Scientist. His research focuses on new navigation methods and nonlinear dynamical systems. He is also a former professor and Air Force Officer. Dr. Ely is the recipient of JPL's Magellan Award and NASA's Outstanding Public Leadership Medal for his work on DSAC.

Dr. Jill Seubert is an interplanetary navigator and a leading expert on astrodynamics, estimation, deep space navigation, and specializes in technology advancements to support the next generation of deep space exploration. In her 10 years as a navigator at NASA's Jet Propulsion Laboratory, she navigated numerous high-profile Mars missions. She most recently served as the Orbit Determination Lead for the Mars Science Mission 2020, guiding it to a safe landing on Mars on February 18, 2021. Dr. Seubert was also the Deputy Principal Investigator and Mission Operations Manager of NASA's successful Deep Space Atomic Clock Technology Demonstration Mission. Dr. Seubert was awarded the 2020 NASA Exceptional Public Achievement Medal for her outstanding leadership of the Deep Space Atomic Clock mission. She has been honored as the recipient of the University of Colorado College of Engineering Recent Alumni Award (2017) and Pennsylvania State University "40 Under 40" award (2021). She holds a B.S. degree in Aerospace Engineering from the Pennsylvania State University and M.S. and Ph.D. degrees in Aerospace Engineering Sciences from the University of Colorado at Boulder.

Dr. John Prestage is a senior scientist at JPL. He recently led the prototype flight mercury ion-trap atomic clock effort to bring Hg ion clock technology to the TRL 5 in a package suitable for long duration space navigation missions. This work was the basis and starting technology for the NASA Technology Development Mission Deep Space Atomic Clock (DSAC), for which he is a co-investigator. He received a Ph.D. in atomic physics from Yale University in 1983 followed by 2 years of postdoctoral work in the ion storage group at NIST, Boulder participating in development of the first ever laser cooled atomic clock. Since coming to JPL, he developed the first linear quadrupole rf ion trap, the first multi-pole linear ion trap together with ion shuttling to enable ultra-stable atomic ion clock for continuous operation. He also developed the first 10^{-15} frequency stable, sealed vacuum tube-based ion clock, making an essential technology advance for a compact ion-clock. Recently, he has miniaturized ion-clock physics package architectures to few cubic centimeters for both DARPA IMPACT and ACES recent efforts. He has been awarded nearly 20 NASA new Technology awards, 3 Patents, and a NASA Exceptional Technology Achievement Medal, and the 2009 IEEE I. I. Rabi Award for Ion trap Atomic Clock development and fundamental physics investigations via atomic clock frequency comparisons.

Dr. Robert L. Tjoelker has been at the NASA Jet Propulsion Laboratory since 1990. For the last two decades he was Technical Supervisor of JPL's Frequency and Timing Advanced Instrument Development Group responsible for frequency and timing research and development for the NASA Deep Space Network (DSN) and spaceflight. He's made multiple contributions to the realization of practical, ultra-stable trapped mercury ion clocks, including clock systems developed for NASA and the DoD. Since 2011, He has been the Ion Clock Co-Investigator for the NASA's

Deep Space Atomic Clock Mission. Dr. Tjoelker has published more than 100 papers in the areas of fundamental constants and atomic physics, precision trapped ion mass spectrometry, atomic frequency standards, and frequency and timing systems. He is a member of the IEEE Ultrasonics, Ferroelectrics, and Frequency Control Society, the American Physics Society, the International Telecommunication Union USWP-7A, and has served multiple roles with the ION Precise Time and Time Interval Systems and Applications Meeting (PTTI), and the IEEE International Frequency Control Symposium. Robert L. Tjoelker received degrees in architecture, physics, and mathematics from the University of Washington and the Ph.D degree in physics from Harvard University, for a precision comparison of the proton and antiproton mass.

Dr. Eric Burt received a B.S. degree in mathematics from the University of Michigan, and a Ph.D. in physics from the University of Washington. His Ph.D. thesis was on the trapping and laser-cooling single indium ions. From 1995 to 1997 he was a postdoctoral fellow at the University of Colorado, working with Carl Wieman on experiments with Bose-Einstein condensates including dual-species condensates and the demonstration of higher-order coherence in condensate atoms. From 1997 to 2001 he worked at the U.S. Naval Observatory developing a laser-cooled cesium fountain atomic clock. From 2001 to the present, he has worked at the Jet Propulsion Laboratory (JPL), California Institute of Technology where he is currently Principal Member of Technical Staff. His work at JPL has included development of both ion and laser-cooled neutral atomic clocks. Dr. Burt is a senior member of the IEEE, current co-general chair for the IEEE Frequency Control Symposium, and Secretary/Treasurer for the APS Topical Group on Precision Measurement and Fundamental Constants. He is the recipient of the 2015 NASA STMD Groundbreaker award and the 2020 NASA Exceptional Technology Achievement Medal for his work on space atomic clocks.

Dr. Angie Dorsey is an aerospace engineer working at NASA's Jet Propulsion Laboratory in Pasadena, California. She received her BS in Aerospace Engineering from the University of Alabama and a Ph.D. in Aerospace Engineering Sciences from the University of Colorado Boulder. She works in the area of high precision, space borne GNSS receivers for use in scientific applications.

Dr. Daphna G. Enzer received the S.B. degree in physics from Yale University, New Haven, CT, USA, in 1989, and the A.M. and Ph.D. degrees in atomic physics from Harvard University, Cambridge, MA, USA, in 1991 and 1996, respectively. Her Ph.D. thesis focused on the quantum to classical transition of a single electron in a Penning trap. After a one-year post-doctoral fellowship at Harvard University, she spent two years as a Director's Post-Doctoral Fellow at Los Alamos National Laboratory working on quantum computing with trapped calcium ions and quantum cryptography with polarization entangled photon pairs. She joined the NASA Jet Propulsion Laboratory, California Institute of Technology, Pasadena, CA, USA, in 2001, and is currently a member of the Frequency and Timing Advanced Instrument Development Group. Her interests include precision measurement instruments, both development and data analysis, with contributions to: cold atom cesium fountain and space clock prototype development; Gravity Recovery and Interior Laboratory (GRAIL) mission radio link performance analysis; and JPL frequency stability measurement-system development, algorithm, and performance analysis. She is currently leading mercury ion-clock system-modeling activities and actively engaged in the flight-operations team for the Deep Space Atomic Clock (DSAC) Mission. Dr. Enzer is a member of the American Physical Society.

Randy G. Herrera is the deputy section manager of the Project Systems Engineering & Formulation section (312) at NASA's Jet Propulsion Laboratory (JPL). He graduated from Texas A&M University (B.S.) in 1985 and Rensselaer Polytechnic Institute (M.S.) in 1988 with degrees in electrical engineering. He has received numerous awards in his career at JPL including NASA's Exceptional Achievement Medal, the JPL Award for Excellence, and JPL's People Leadership Award. Over the last 30 years, he has participated in the review of more than 40 proposals and has been the Project Systems Engineer (PSE) for NASA Class-D missions Cold Atom Laboratory (CAL) and Deep Space Atomic Clock (DSAC), covering the gamut of mission development from initial conceptualization to launch and operations.

Dr. Da Kaung received his Ph.D. degree in Aerospace Engineering from The University of Texas at Austin in 1995. He joined NASA's Jet Propulsion Laboratory in 1996 and is a senior research technologist in Near Earth Tracking Application Group. He has worked on precise orbit determination for GNSS satellites, as well as using GNSS tracking data for LEO satellites orbit determination. His experience

includes satellite surface force modeling, measurement geometry modeling and clock modeling for GPS, GLONASS, SRTM, CHAMP, SAC-C, GRACE, COSMIC, PAZ and some other remote sensing LEO satellites. He has been a member of AGU and ION for more than 25 years.

Dr. David Murphy received the B.A. degree (Hons.) in physics from the University of Cambridge, Cambridge, U.K., in 1983, and the Ph.D. degree in physics from The University of Manchester, Manchester, U.K., in 1988. His Ph.D. in physics (radio astronomy) was on VLA observations of core-dominated quasars. From 1987 to 1988, he was a Research Associate with The University of Manchester. From 1989 to1990, he was a National Research Council Post-Doctoral Associate at the Jet Propulsion Laboratory (JPL), California Institute of Technology, Pasadena, CA, USA. In 1991, he became a member of JPL's Astronomical Measurements Group, and in 2006 its Group Supervisor. From 1991 to 2011, he was involved in both the Japanese VSOP and the Russian RadioAstron Space VLBI missions and NASA's Space Interferometry Mission and Kepler mission. In 2011, he joined the Deep Space Atomic Clock (DSAC) Project and in 2012 became the Group Supervisor of the Near Earth Tracking Applications Group. His DSAC mission work involves using the data from the on-board GPS receiver to determine the Allan Deviation of the DSAC clock.

David Robison is a member of the GNSS and Signals of Opportunity Flight Instruments group at NASA's Jet Propulsion Laboratory, specializing in instrument development, digital signal processing, and FPGA design. He received his B.S. and M.Eng. in Electrical Engineering and Computer Science from the Massachusetts Institute of Technology in 2000 and 2001, respectively. He has contributed to numerous flight GNSS receivers, including those flown on OSTM, JASON-3, COSMIC, and COSMIC-2, and has also held lead FPGA and software roles for the Moon Mineralogy Mapper instrument and the Deep Space Atomic Clock. He is currently the instrument system engineer for the SunRISE project.

Gabriella (Ella) Seal is a mechanical reliability and environmental requirements engineer at the Jet Propulsion Laboratory, where she has worked since obtaining her B.S. in Mechanical Engineering from the California Institute of Technology in 2013. Experience and projects include instrument assembly/integration/test engineering for Deep Space Atomic Clock (DSAC), mission assurance management for Surface Water and Ocean Topography (SWOT), and mechanical reliability and environmental requirements engineering for Mars 2020 and Europa Clipper.

Dr. Jeffrey Stuart is a GNC Engineer in the Mission Design and Navigation Section at the Jet Propulsion Laboratory, where he works across all phases of mission development and operations. His experiences include MDNav Lead for the SunRISE formation flying radio interferometer as well as orbit determination for the Deep Space Atomic Clock. He received his Ph.D. (2014), M.S. (2011), and B.S. (2008) from the School of Aeronautics and Astronautics at Purdue University.

Dr. Rabi Wang obtained a PhD in Superfluidity from University of Oregon in 1987. After two years of postdoc work with National Research Council, he joined JPL research staff for the cryogenic sapphire oscillator project. He worked on several JPL flight projects including GRAIL, Grace-follow-on, Insight, and DSAC. Currently he is the subsystem engineer for the Deep Space Network Frequency and Timing system.